

Surfing and crawling macroscopic active particles under hard confinement – inertial dynamics

Marco Leoni,^{1,*} Matteo Paoluzzi,^{2,*} Sarah Eldeen,³ Anthony Estrada,³ Lauren Nguyen,⁴ Maria Alexandrescu,⁵ Karin Sherb,⁵ and Wylie W. Ahmed^{3,†}

¹*Université Paris-Saclay, CNRS, IJCLab, 91405, Orsay, France*

²*Institute of Complex Systems (ISC-CNR) and Department of Physics, Sapienza University of Rome, Italy*

³*Department of Physics, California State University Fullerton, CA 92831 USA*

⁴*Department Chemistry and Biochemistry, California State University Fullerton, CA 92831 USA*

⁵*Troy High School, Fullerton, CA 92831 USA*

(Dated: May 15, 2022)

We study two types of active (self-propelled) macroscopic particles under confinement: camphor surfers and hexbug crawlers, using a combined experimental, theoretical, and numerical approach. Unlike widely studied microscopic active particles and swimmers, where thermal forces are often important and inertia is negligible, our macroscopic particles exhibit complex dynamics due expressly to active non-thermal noise combined with inertial effects. Hard confinement induces accumulation at a finite distance *within* the boundary and gives rise to three distinguishable dynamical states; both depending on activity and inertia. These surprisingly complex dynamics arise already at the single particle level — highlighting the importance of inertia in macroscopic active matter.

Introduction. Active matter is a rapidly growing field of research that studies the behavior of self-driven entities that exhibit rich dynamics and collective phenomena in systems covering a wide range of length scales [1–3]. This ranges from molecular-scale systems such as driven biopolymers [4] up to meter-scale systems like dense crowds of people [5–7]. Physical confinement of active systems, critical not only to understand the effect of boundaries but also for applications to real-life systems, triggers interesting dynamical behaviors, e.g. collective motion, accumulation, segregation, phase separation, and freezing/fluidization [8–15]. While experimental observations in starling flocks have shown the importance of inertial effects in flocking transitions [16], how inertia modifies some peculiar features of active systems, such as accumulation at the boundaries or anomalous density fluctuations remains unknown.

For a system in thermal equilibrium the density follows the Boltzmann distribution [17]. This means, for instance, that a Brownian particle under confinement will uniformly explore the space, without developing currents. In stark contrast, systems of active particles exhibit a steady-state density profile with an accumulation peak at the confining wall [12, 18–21] as it has been observed in experiments [9, 15]. Most studies have focused on overdamped systems due to the ubiquity of experimental work at the microscopic scale [3], however, a growing number of experimental observations highlight the importance of inertia in macroscopic active matter systems [21–25].

In this *letter* we study the role of a hard confining

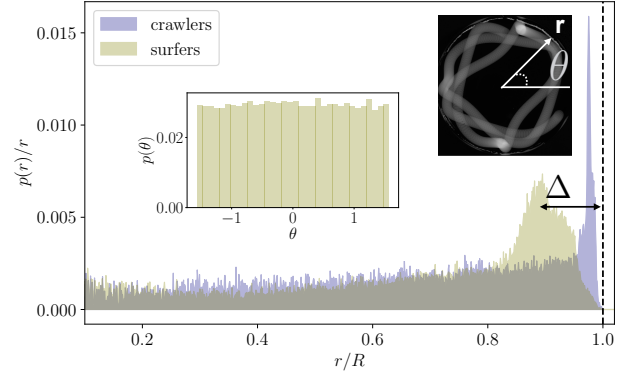


FIG. 1: Probability distribution of the position of an isolated active particle in presence of hard boundaries for camphor surfers (green) and hexbug crawlers (violet). These distributions are peaked at a distance Δ within the system boundary (dashed vertical line), unlike in overdamped systems. Insets: a representative angular probability distribution (left, units in radians) and a time-lapse of a surfer's trajectory (right).

boundary on the dynamics of macroscopic active particles, at two length scales (mm and cm) where inertia is non-negligible. We use two different systems, comprising both wet and dry active matter: camphor surfers, which glide at the fluid air interface via a surface tension-driven motion [26]; and Hexbug crawlers, which are propelled on a solid surface by a vibrating motor [21]; hereafter, referred to as surfers and crawlers. Strikingly, due to the interplay of inertial dynamics and hard confinement we observe rich dynamics already at the single particle level. We observe: (1) steady-state density distributions that exhibit an accumulation peak at a finite distance *within* the confining wall, and (2) transitions between three dynamical states that we call “orbits”, “epicycles”, and “collisions”. Through experiments, modeling, and

*equally contributing authors

†correspondence: wahmed@fullerton.edu

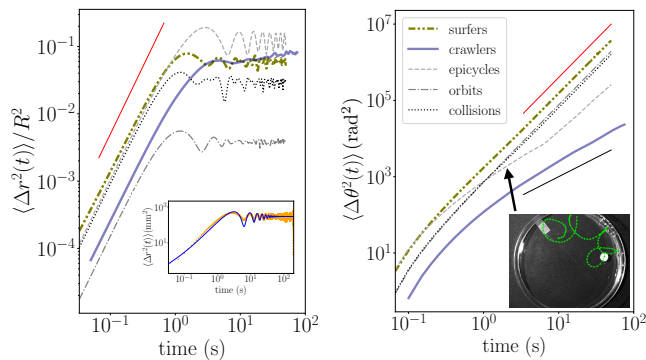


FIG. 2: Mean square displacements (MSDs). Left: MSD for the radial coordinate, $r(t)$, normalized to the container size, R . A crossover from ballistic to a flat plateau indicates confinement. In most experimental runs oscillatory behaviour is observed (inset, shows theoretical fit for surfers). From this we estimate $m/\gamma \sim 40$ and 5 s for surfers and crawlers, respectively. Right: MSD for the angular coordinate $\theta(t)$. The angular dynamics is consistent with ballistic motion in surfers and diffusive motion for crawlers. Kinks, describing multiple timescales, are observed e.g. during epicycles (inset). Power laws of ballistic (solid red) and diffusive (solid black) dynamics are shown as a guide for the eye.

simulations we show that the self propulsion speed of the inertial active particles controls the location of the density peak and drives transitions between the three dynamical states. Including inertia in models is critical in capturing the observed dynamics.

Materials and Methods Experiments consist of two separate systems: (1) Millimeter-scale camphor surfers were created by infusing agarose gel disks with camphor solution as studied previously [26, 27]. The resulting self-propelled surfer has a radius of ~ 3 mm. The dynamics is then studied by placing the surfer at the water-air interface in a circular petri dish of 10 cm diameter with 20 g of ultrapure water. Self-propulsion is driven by gradients in surface tension. (2) Centimeter-scale crawlers were created using a Hexbug nano [21] that is trapped under a rigid isotropic container of radius ~ 3 cm. The crawler is then placed on a flat circular table of ~ 1 m diameter that has a vertical wall around its edge. Self-propulsion is driven by a mechanical vibrating motor. Thus these two systems comprise wet and dry active matter systems and differ in scale by an order of magnitude. For both systems motion was recorded at 20-30 Hz. See SM for details.

Spatial distributions and MSD. First, we focus on the average properties of active particles interacting with the boundaries in presence of both inertia and friction. To characterize the statistical behaviour of the system, we tracked the positions (using custom code written in MATLAB), computed the polar coordinates $\mathbf{r}(r, \theta)$ with origin at the center of the container, and calculated the probability distributions of their positions, $p(r)$ and

$p(\theta)$ (Fig.1). As expected $p(\theta)$ shows a uniform distribution because the containers are rotationally symmetric about their origin. The uniform distribution in angle likely arises from the rotating dynamics of particles along the boundary of the container, see below for details, but is also consistent with random motion. Interestingly, the radial distribution, $p(r)$, of these active particles under confinement is new: it is not uniform, as one might expect in the case of Brownian particles, nor peaked at the boundary, as it was found for active Brownian particles — e.g. micro-swimming bacteria [9]. Instead, here, the most probable configuration is at some finite distance *within* the boundary of the container as shown in Fig.1 by Δ . This observation, along with our analytic and numerical models showing Δ depends on persistence, is the first main result of our *letter*.

To gain insight on this behaviour, we computed the radial and angular mean squared displacement (MSD), as shown in Fig.2. For both surfers and crawlers the radial MSD initially grows ballistically in time followed by a crossover to a flat plateau as expected for the motion of a particle confined to a circular region. Often oscillations are observed for surfers in the crossover region Fig.2(left). The angular displacement instead is simpler: typically ballistic for surfers and nearly diffusive for crawlers. Sometimes kinks and crossovers between two regions with similar slope are observed. We interpret these as signatures of a multi-scale dynamics: for instance local rotational motion — Fig.2(right), see inset — followed by an overall large scale rotation along the boundary.

An important difference with respect to microscopic systems is that these particles are too large to be sensitive to thermal fluctuations. However, we still observe noise, e.g. fluctuations in positions and in the speed. Surfers provide an example of a macroscopic non-thermal suspension where fluctuations are active in origin, and when activity is absent (e.g. the camphor is exhausted), then the noise is also absent. Crawlers are similar where the activity/noise comes from the vibrating motor. From our measurements, the speed fluctuations have Gaussian behaviour when the particle is far from the boundaries of the system (Fig.3). Collisions and interactions with the boundary result in a distribution of speeds near the boundary which has large tails in the case of surfers, but which is qualitatively similar to the bulk distribution for crawlers. Presumably for crawlers this is due to the fact that the collisions with the container are mediated by the surrounding isotropic cup, which is present also when particles are far from the boundaries and could be responsible for a similar randomization of the speed both in the bulk and close to boundaries as shown in Fig.3.

Analytical model. To gain insight we examine a simple model similar to active Brownian particles (ABP) with inertia. We consider a particle centered at position \mathbf{x} . Then $\dot{\mathbf{x}} = \mathbf{v}$ is the particle's velocity whose dynamics is

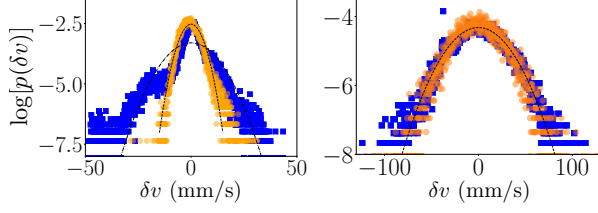


FIG. 3: Distribution of speed fluctuations, δv (where $\delta v = v - \langle v \rangle$ and $v = |\mathbf{v}|$), for surfers (left) and crawlers (right). Blue squares and orange circles indicate near boundaries and in the bulk, respectively. Fluctuations in the bulk (orange) look nearly Gaussian, while the near the boundary (blue) non-Gaussian tails are evident, particularly for surfers (left). Dashed and dotted-dashed lines show Gaussian distributions with experimental variance.

described by

$$m\dot{\mathbf{v}} = -\gamma(\mathbf{v} - \mathbf{v}_0) - \hat{\mathbf{r}} \frac{\partial U}{\partial r}. \quad (1)$$

Here \mathbf{v}_0 is the active velocity which includes both deterministic and fluctuating terms. This is the main difference from the usual ABP model [28]: in our system there are no thermal fluctuations and the noise is directly linked to the activity. This is sometimes referred to as active Langevin motion [29]. $\hat{\mathbf{r}} \frac{\partial U}{\partial r}$ is the force (U is the potential) acting on the radial direction, $\hat{\mathbf{r}}$, due to confinement. Writing the particle position \mathbf{x} in polar coordinates as $\mathbf{x} = r(\cos \theta, \sin \theta)$, then $\hat{\mathbf{r}} = \mathbf{x}/r$. To compute the radial MSD we use the simplest model to describe the boundary effect: a harmonic potential $U = kr^2/2$ (see numerical simulations for hard confinement). The velocity vector $\dot{\mathbf{x}}$ is written $\dot{\mathbf{x}} = \dot{r}\hat{\mathbf{r}} + r\dot{\theta}\hat{\boldsymbol{\theta}}$ and the acceleration $\dot{\mathbf{v}} = (\ddot{r} - r\dot{\theta}^2)\hat{\mathbf{r}} + (2\dot{r}\dot{\theta} + r\ddot{\theta})\hat{\boldsymbol{\theta}}$. The radial and angular equations are obtained by projecting Eq.(1) onto $\hat{\mathbf{r}}$ and $\hat{\boldsymbol{\theta}} = (-\sin \theta, \cos \theta)$ respectively. We note that these equations are coupled if inertia is non-negligible, $m \neq 0$. Projecting the equation on the radial direction, we write the active speed $(\mathbf{v}_0 \cdot \hat{\mathbf{r}}) = v_0(1 + \xi(t))$ as the sum of two terms: a constant part, v_0 , and a fluctuating part, $\xi(t)$, which has zero mean and correlations $\langle \xi(t)\xi(t') \rangle = \Lambda \delta(t - t')$. Λ describes the strength of fluctuations in the radial velocity, which has a non-thermal origin that can be related to fluctuations in the activity due to chemical reactions for the surfers or the vibrating motor for the crawlers, see Fig.3.

To study the radial MSD, for simplicity we assume constant angular dynamics, $\dot{\theta} = \Omega$. This represents an overall rotational motion, as often observed in experiments (see Fig.4), and allows us to decouple the radial equation from the angular one, obtaining $m\ddot{r} = -\gamma\dot{r} + \gamma v_0 + \gamma v_0 \xi(t) - m\omega_0^2 r$ where $\omega_0^2 = k/m - \Omega^2$. This result is the classical equation of the Brownian oscillator [30]. The radial MSD is computed (once we subtract

the average contribution) from the relation $\langle \Delta r^2(t) \rangle = \langle [r(t) - r(0)]^2 \rangle = 2\langle r^2 \rangle - 2\langle r(t)r(0) \rangle$. We obtain,

$$\langle \Delta r^2(t) \rangle = 2\gamma^2 v_0^2 \frac{\Lambda}{m\omega_0^2} \times (1 - e^{-2\frac{\gamma}{m}t} [\cos(\omega_1 t) + \frac{\gamma}{2m\omega_1} \sin(\omega_1 t)]) \quad (2)$$

where $\omega_1^2 = \omega_0^2 - \frac{\gamma^2}{4m^2}$

The fit reproduces the experimental data accurately for surfers, see the inset of Fig.2. The oscillations near the plateau could be related to the bouncing dynamics of the particles near the boundary — which only occurs in the presence of inertia. In the case of surfers, the fit yields the values $m/\gamma \sim 40$ s, $\omega_1 = 189.48$ rad/s, and a plateau of ≈ 300 mm². For crawlers, we obtain $m/\gamma \sim 5$ s, and a plateau of ≈ 15000 mm², with no appreciable oscillations ($\omega_1 \approx 0.6$ rad/s) see violet curve of Fig.2(left). This suggests that in our setup inertia plays a stronger role for surfers than crawlers.

How a simple model approximating the confining boundary as a harmonic potential fits the data for both surfers and crawlers is not entirely clear. For surfers, presumably interactions with the boundary of the container are mediated by capillary forces (a meniscus is visible in the proximity of the boundary) [31]. To first approximation, a spring-like potential could represent the meniscus force felt by the particle when colliding. A similar effect can be envisaged for the crawlers for interactions of the isotropic cup and container wall. A difference worth noting is that because the particles are actively driven, the oscillations (albeit damped) do not vanish in the radial MSD.

The equation for the angular coordinate is $m r \ddot{\theta} = -(\gamma r + 2m\dot{r})\dot{\theta} + \nu(t)$ where $\nu(t)$ represents noise, which in the simplest case is zero except at the instant of collision with the boundary. As we see, the equation is still coupled to the radial position. To decouple these variables, we write $r(t) \approx r_0$, which represents some average radial position (e.g. the peak of the distribution in Fig.1). Hence, the equation for the angle is $\ddot{\theta} = -\frac{\gamma}{m}\dot{\theta} + \frac{\nu(t)}{mr_0}$. The solution for the angle in this case is obtained by considering delta-correlated noise $\langle \nu(t')\nu(t'') \rangle = \Gamma \delta(t' - t'')$, as $\langle \Delta \theta^2 \rangle \approx \Omega^2 t^2$ in the regime where inertia dominates [32]. If we neglected m , following the same calculation the angular MSD would become diffusive, $\langle \Delta \theta^2 \rangle \approx \frac{\Gamma}{\gamma^2 r_0^2} t$ with Γ the strength of fluctuations in angular velocity. Together, this analysis suggests the surfers exhibit strong inertial effects because of the ballistic angular dynamics and oscillations in radial dynamics, while the inertial effects of our crawlers [36] is less apparent — consistent with the m/γ extracted from the radial analysis.

Dynamical transitions between states. So far we have discussed statistical properties of these single particle systems. However, this does not distinguish finer dynamical features that are associated with a particle's indi-

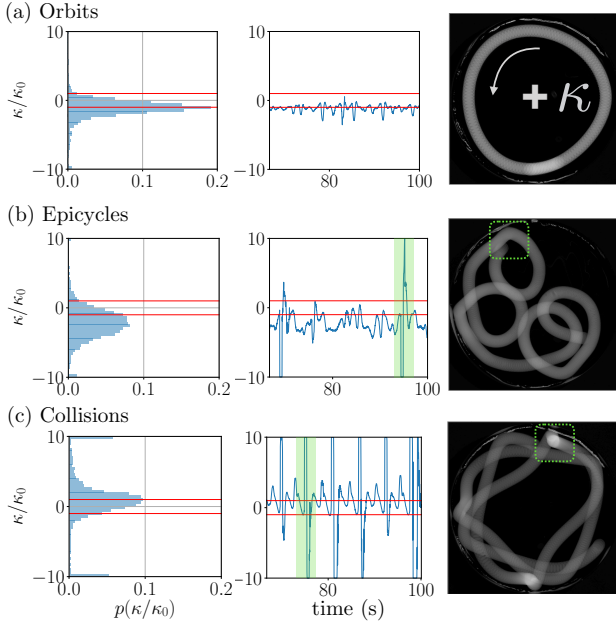


FIG. 4: Characterization of different dynamical states: (a) orbits, (b) epicycles, and (c) collisions. The left-column shows the distribution of the curvatures. Curvatures are truncated at the value $10\kappa_0$, where $\kappa_0 = 1/R$ is the container curvature. The horizontal red lines indicate the boundary curvature, $\kappa = \pm\kappa_0$. The middle-column shows the curvature as a function of time, corresponding to the time-lapse trajectories shown in the right-column. A κ/κ_0 value of zero indicates motion in a straight line. (a) Orbiting dynamics exhibit a sharp peak at the curvature corresponding to the boundary, $|\kappa_0|$. (b) Epicycles exhibit a wider distribution of curvatures peaked at a higher value, $\approx |2\kappa_0|$, indicating “sharper” turns. (c) Collisions exhibit more complex dynamics, with a central peak in curvature similar to the container’s boundary, and two large shoulders at very high curvature, $\pm 10\kappa_0$, associated with collisions where abrupt changes in direction take place. Shaded green regions in the time dynamics (middle-column) correspond to abrupt changes in curvature indicated in trajectories (right-column).

vidual trajectory. By focusing on such dynamical details, we find three states: (1) *Orbits*, where particles move, approximately, on circular trajectories with curvature similar to the size of the hard confining boundary. (2) *Epicycles*, where rotation at small scales is coupled to rotation along the container’s boundary; (3) *Collisions*, where relatively straight trajectories are followed by abrupt changes in direction due to the collisions with the boundary. While orbits have been observed in soft confinement [21], the richer dynamics of epicycles and collisions are unique. This observation, along with our numerical model suggesting transitions between dynamical states is tuned by activity, is the second main result of our *letter*.

These three dynamical states are shown for surfers in Fig.4, and transitions between them are possible. Signatures of these dynamical states also emerge in the

MSDs shown in Fig.2. While all three states have ballistic dynamics at short times, they exhibit different plateau values in the radial dynamics at longer times – *epicycles* exploring the largest radial area, followed by *collisions* which typically avoid the center of the container, and finally *orbits* where particles typically stay in a small region near the boundary Fig.2(left). These dynamics are also visible in the angular MSDs where *orbits* and *collisions* have the fastest angular motion, and *epicycles* exhibit multi-scale dynamics with comparable motion at short-times but a transition to a slower overall angular motion at long-time due to the local rotations Fig.2(right). These dynamics are also visible in the representative timelapse trajectories shown in Fig.4(right). In crawlers, we see similar states and transitions between, however, less pronounced. This suggests that inertia plays a key role in the observed dynamical states.

The local curvature $\kappa(t)$ along the particle trajectory provides a convenient way to characterize the dynamical features. The curvature is computed from the (x, y) coordinates of the particles using a standard 2D formula: $\kappa(t) = \frac{(\dot{x}\ddot{y} - \dot{y}\ddot{x})}{(\dot{x}^2 + \dot{y}^2)^{3/2}}$. In interpreting these dynamics, $\kappa(t) > 0$ corresponds to a counter-clockwise motion and $\kappa(t) < 0$ clockwise. Asymmetry in the distribution of κ/κ_0 , for a single trajectory arises due to persistent rotational motion in one direction (κ_0 is the container curvature). In Fig.4 we show a curvature dynamics for our three dynamical states. The *orbits* state (Fig.4a) is the most straightforward, exhibiting a single relatively narrow peak at a value of $|\kappa/\kappa_0| \approx 1$ because the surfer is consistently undergoing rotational motion along the boundary. The *epicycles* state (Fig.4b) is mainly characterized by a single large and wide peak. The peak is wide and biased towards larger values of $|\kappa/\kappa_0|$ due to multi-scale rotational dynamics, and thus a wider distribution of curvatures. The *collisions* state (Fig.4c) is characterized by two large peaks at $\pm 10\kappa_0$ that correspond to collisions with the boundary generating high-curvature turns and a third more central peak at $\approx |\kappa_0|$ due to overall rotating dynamics near the boundary reminiscent of orbits. It is worth noting there is always an overall rotational motion (i.e. non-zero peak in κ/κ_0 and ballistic angular MSD). This means an active particle with non-negligible inertia in a rotationally symmetric container generates persistent rotational motion in one direction. This is an example of spontaneous breaking of rotational symmetry at the single particle level.

Numerical simulations. Our simulations show that the dynamical states observed in experiments can be rationalized in terms of a simple model of an active Langevin disc in the underdamped regime [22, 29]. This goes beyond the analytical model described above, by including the dynamic inertial equation for the disc’s orientation, \mathbf{n} , and introducing a “hard” confining boundary (see sup-

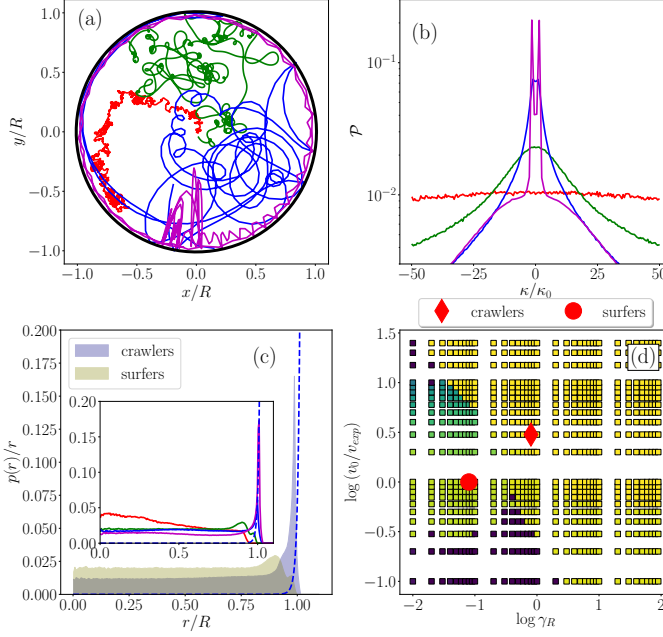


FIG. 5: Numerical simulations. (a) Representative trajectories of the numerical model for $v_0/v_{exp} = 0.1, 1, 10, 100$ (red, green, blue, and magenta respectively). (b) Distribution of local curvatures $\mathcal{P}(\kappa/\kappa_0)$, averaged over many trajectories. (c) The radial distribution function with parameters suitable for reproducing surfers and crawlers. Inset corresponds to velocities in (a,b). (d) A phase diagram of the position of the peak in the radial distribution function (yellow corresponds to $r/R = 1$, violet is $r/R = 0$). Crawlers (red diamond) exhibit a single peaked distribution within but near the boundary. Surfers exhibit a peak well within the boundary with a depletion region near the wall.

plement for details). In the numerical model, a disc of radius a and mass m moves confined in a circular container of radius R . The disc experiences a self-propulsive force along the direction \mathbf{n} that causes a self-propulsive velocity of magnitude v_0 . Because of its finite size, the disc is also characterised by its moment of inertia I . The orientation \mathbf{n} is subjected to a random and uncorrelated noise whose fluctuations are characterized by a rotational diffusion constant D_r .

Fig.5a shows four representative trajectories at different self-propulsion velocity $v_0/v_{exp} = 0.1, 1, 10, 100$ and fixed $\gamma_R/\gamma = 8 \times 10^{-2}$ (the ratio has been chosen to describe the surfers). v_{exp} is the typical scale of velocity measured in experiments. As the velocity increases, trajectories transition from Brownian-like to richer dynamical features of *epicycles*, *collisions*, and *orbits*. This is an indication that the presence of different regimes observed in experiments may be due to the magnitude of the self-propulsion velocity, i.e., an observable that is not directly accessible in experimental measurements. We look at the statistical distribution of local curvatures $\mathcal{P}(\kappa)$ as shown in Fig.5b. At small velocities, trajectories

are almost Brownian and the distribution is flat (red). As v_0 increases, ballistic dynamics give rise to a peak at $\kappa = 0$ (green). When epicycles dominate the dynamics, \mathcal{P} develops a shallow double-peaked structure (blue). The double peak is due to averaging over a large number of trajectories, where in each simulation the disc may be persistently rotating in the positive or negative κ direction. This persistent rotation emerges where collisions with the boundary are observed (blue) at intermediate activity but at higher activity orbits dominate and exhibit a deep double-peaked structure (magenta) as shown in Fig.5a,b.

To compare the numerical model with the experiments we look at the steady-state properties through the radial distribution function (using simulation parameters compatible with experiment). The result, shown in Fig.5c, is in fair agreement with the experiment. Namely that both surfers and crawlers show an accumulation at a finite distance, Δ , within the container boundary, and that this effect is stronger with increasing influence of inertia (e.g. surfers vs crawlers). Finally, using as a criterion the distance from the boundaries, we develop a phase diagram (Fig.5d). The color map indicates the position of the peak of the radial distribution function r_{peak} . Yellow indicates that $r_{peak}/R = 1$, violet indicates $r_{peak}/R = 0$. The violet region suggests the distribution becomes flat. As one can see, as the inertial effects become negligible (large γ_R values), the peak is located at the boundary (yellow) regardless of the self-propulsion speed, as already observed in other experiments [9, 15]. However, when inertia dominates (at lower values of γ_R), the phase diagram shows rich behavior as the self-propulsion speed is varied. Very low v_0 shows uniform distributions (violet) as expected for Brownian motion, and higher v_0 show a peak of the distribution at a finite distance within the boundary (shades of green), Δ , as observed in our experiments — e.g. *epicycles* and *collisions* tend to move the peak away from the boundary.

It is worth noting that the structure of the radial distribution function shows richer features than in the overdamped case [9]. This is made evident by the green regions in the phase diagram (upper-left) where the peak of the distribution not only moves away from the boundary, but it also exhibits a depletion region close to the wall — visible in Fig.5c. This observation is in agreement with experiments, most visibly in surfers (green curve in Fig.1) that exhibit a peak at finite distance Δ from the boundary. Moreover, the distributions in both experiments and simulations exhibit a “shoulder” in the depletion region (green curves in Fig.1 and Fig.5c).

Conclusions. To summarize — In “hard” confinement a Brownian particle will uniformly explore the space; and an overdamped active particle will accumulate at the container wall. In this *letter*, we show that a self-propelled particle with non-negligible inertia gives rise to two new effects: (1) Particles accumulate at a finite

distance *within* the container wall, and this distance increases with activity and inertia. (2) Three dynamical states (and transitions between them) are observed that can be characterized by the local curvature, all of which include breaking of rotational symmetry. Both (1) accumulation and (2) transitions between dynamical states can be tuned by activity, v_0 , and only exist when inertia is non-negligible. These observations open a new avenue for inertial active matter, because they show that, thanks to inertial effects, active particles can be spatially sorted in target regions by varying the properties of the particle itself without introducing an external field or opportune sculptured environments [33, 34]. Further modeling and experiments are necessary to fully understand the role of inertia on the spatial distribution of active particles, the finer features of their dynamical states, and how this affects multi-particle interactions.

Acknowledgments.— MP acknowledges funding from Regione Lazio, Grant Prot. n. 85-2017-15257 ("Progetti di Gruppi di Ricerca - Legge 13/2008 - art. 4"). SE and AE acknowledge the Black Family Fellowship. WWA acknowledges funding from CSUF RSCA and iREU NSF Grant No. 1560390.

-
- [1] M Cristina Marchetti, Jean-François Joanny, Sriram Ramaswamy, Tanniemola B Liverpool, Jacques Prost, Madan Rao, and R Aditi Simha. Hydrodynamics of soft active matter. *Reviews of Modern Physics*, 85(3):1143, 2013.
 - [2] Sriram Ramaswamy. The mechanics and statistics of active matter. *Annu. Rev. Condens. Matter Phys.*, 1(1):323–345, 2010.
 - [3] Clemens Bechinger, Roberto Di Leonardo, Hartmut Löwen, Charles Reichhardt, Giorgio Volpe, and Giovanni Volpe. Active particles in complex and crowded environments. *Reviews of Modern Physics*, 88(4):045006, 2016.
 - [4] Tim Sanchez, Daniel TN Chen, Stephen J DeCamp, Michael Heymann, and Zvonimir Dogic. Spontaneous motion in hierarchically assembled active matter. *Nature*, 491(7424):431, 2012.
 - [5] Nicolas Bain and Denis Bartolo. Dynamic response and hydrodynamics of polarized crowds. *Science*, 363(6422):46–49, 2019.
 - [6] Arianna Bottinelli, David TJ Sumpter, and Jesse L Silverberg. Emergent structural mechanisms for high-density collective motion inspired by human crowds. *Physical review letters*, 117(22):228301, 2016.
 - [7] Jesse L Silverberg, Matthew Bierbaum, James P Sethna, and Itai Cohen. Collective motion of humans in mosh and circle pits at heavy metal concerts. *Physical review letters*, 110(22):228701, 2013.
 - [8] Julien Deseigne, Olivier Dauchot, and Hugues Chate. Collective motion of vibrated polar disks. *Phys. Rev. Lett.*, 105(9):098001, 2010.
 - [9] ID Vladescu, EJ Marsden, J Schwarz-Linek, VA Martinez, J Arlt, AN Morozov, D Marenduzzo, ME Cates, and WCK Poon. Filling an emulsion drop with motile bacteria. *Physical review letters*, 113(26):268101, 2014.
 - [10] Shibbananda Das, Gerhard Gompper, and Roland G Winkler. Confined active brownian particles: theoretical description of propulsion-induced accumulation. *New Journal of Physics*, 20(1):015001, 2018.
 - [11] Lorenzo Caprini, Umberto Marini Bettolo Marconi, and Andrea Puglisi. Activity induced delocalization and freezing in self-propelled systems. *Scientific reports*, 9(1):1386, 2019.
 - [12] J Tailleur and ME Cates. Sedimentation, trapping, and rectification of dilute bacteria. *EPL (Europhysics Letters)*, 86(6):60002, 2009.
 - [13] Yaouen Fily, Aparna Baskaran, and Michael F Hagan. Dynamics of self-propelled particles under strong confinement. *Soft matter*, 10(30):5609–5617, 2014.
 - [14] Xingbo Yang, M Lisa Manning, and M Cristina Marchetti. Aggregation and segregation of confined active particles. *Soft matter*, 10(34):6477–6484, 2014.
 - [15] Sho C Takatori, Raf De Dier, Jan Vermant, and John F Brady. Acoustic trapping of active matter. *Nature communications*, 7(1):1–7, 2016.
 - [16] Alessandro Attanasi, Andrea Cavagna, Lorenzo Del Castello, Irene Giardina, Tomas S Grigera, Asja Jelić, Stefania Melillo, Leonardo Parisi, Oliver Pohl, Edward Shen, et al. Information transfer and behavioural inertia in starling flocks. *Nature physics*, 10(9):691, 2014.
 - [17] Kerson Huang. *Introduction to statistical physics*. Chapman and Hall/CRC, 2009.
 - [18] Caleb G Wagner, Michael F Hagan, and Aparna Baskaran. Steady-state distributions of ideal active brownian particles under confinement and forcing. *Journal of Statistical Mechanics: Theory and Experiment*, 2017(4):043203, 2017.
 - [19] Claudio Maggi, Umberto Marini Bettolo Marconi, Nicoletta Gnan, and Roberto Di Leonardo. Multidimensional stationary probability distribution for interacting active particles. *Scientific reports*, 5:10742, 2015.
 - [20] Umberto Marini Bettolo Marconi, Nicoletta Gnan, Matteo Paoluzzi, Claudio Maggi, and Roberto Di Leonardo. Velocity distribution in active particles systems. *Scientific reports*, 6:23297, 2016.
 - [21] Olivier Dauchot and Vincent Démery. Dynamics of a self-propelled particle in a harmonic trap. *Physical review letters*, 122(6):068002, 2019.
 - [22] Christian Scholz, Soudeh Jahanshahi, Anton Ldov, and Hartmut Löwen. Inertial delay of self-propelled particles. *Nature communications*, 9(1):5156, 2018.
 - [23] Antoine Deblais, Thomas Barois, T Guerin, Pierre-Henri Delville, Rémi Vaudaine, Juho S Lintuvuori, Jean-François Boudet, Jean-Christophe Baret, and H Kellay. Boundaries control collective dynamics of inertial self-propelled robots. *Physical review letters*, 120(18):188002, 2018.
 - [24] Mickael Bourgoin, Ronan Kervil, Cecile Cottin-Bizonne, Florence Raynal, Romain Volk, and Christophe Ybert. Kolmogorovian active turbulence of a sparse assembly of interacting marangoni surfers. *Physical Review X*, 2020.
 - [25] Christian Scholz, Michael Engel, and Thorsten Pöschel. Rotating robots move collectively and self-organize. *Nature communications*, 9(1):1–8, 2018.
 - [26] Dolachai Boniface, Cécile Cottin-Bizonne, Ronan Kervil, Christophe Ybert, and François Detcheverry. Self-propulsion of symmetric chemically active particles:

- Point-source model and experiments on camphor disks. *Physical Review E*, 99(6):062605, 2019.
- [27] Siowling Soh, Kyle JM Bishop, and Bartosz A Grzybowski. Dynamic self-assembly in ensembles of camphor boats. *The Journal of Physical Chemistry B*, 112(35):10848–10853, 2008.
 - [28] Pawel Romanczuk, Markus Bär, Werner Ebeling, Benjamin Lindner, and Lutz Schimansky-Geier. Active brownian particles. *The European Physical Journal Special Topics*, 202(1):1–162, 2012.
 - [29] Hartmut Löwen. Inertial effects of self-propelled particles: From active brownian to active langevin motion. *The Journal of Chemical Physics*, 152(4):040901, 2020.
 - [30] G. E. Uhlenbeck and L. S. Ornstein. *Phys. Rev.*, 36:823, 1930.
 - [31] Satoshi Nakata, Masaharu Nagayama, Hiroyuki Kitahata, Nobuhiko J Suematsu, and Takeshi Hasegawa. Physicochemical design and analysis of self-propelled objects that are characteristically sensitive to environments. *Physical Chemistry Chemical Physics*, 17(16):10326–10338, 2015.
 - [32] Luca Peliti. *Statistical Mechanics in a Nutshell*. Princeton University Press, 2011.
 - [33] Peter Galajda, Juan Keymer, Paul Chaikin, and Robert Austin. A wall of funnels concentrates swimming bacteria. *Journal of bacteriology*, 189(23):8704–8707, 2007.
 - [34] N Koumakis, A Lepore, C Maggi, and R Di Leonardo. Targeted delivery of colloids by swimming bacteria. *Nature communications*, 4(1):1–6, 2013.
 - [35] M. Paoluzzi, R. Di Leonardo, and L. Angelani. Self-sustained density oscillations of swimming bacteria confined in microchambers. *Phys. Rev. Lett.*, 115:188303, Oct 2015.
 - [36] This is not a fundamental difference between crawling vs. surfing. Other choices of model systems considering different crawlers could yield larger m/γ .

Supplemental Materials: Surfing and crawling macroscopic active particles under hard confinement – inertial dynamics

IMAGE CAPTURE AND ANALYSIS

Representative images of a camphor surfer and hexbug crawler are shown in Fig.S1, where the dotted line indicates the container boundary. In both experiments the container was painted with anti-reflective black paint to enhance contrast and images were captured using identical CMOS cameras (Basler acA3088-57um, from Graftek Imaging) where 4x pixel binning was used at the time of acquisition resulting in an image of 768x516 pixels as saved as individual TIFF files. A different lens for each type of experiment was used to accommodate the difference in scale: (1) Computar M3Z1228C-MP for surfers and (2) Kowa LMVZ4411 for crawlers — both purchased from Graftek Imaging. Captured image sequences were analyzed in MATLAB to determine particle trajectories using a custom-written image processing code. Briefly, images were thresholded and background noise was removed via filtering, and the centroid of the single particle was recorded for each frame. Working with single macroscopic particles that remain in-plane and exhibit large contrast with their background is relatively straight-forward and thus the centroid of the particle could be consistently determined in every single frame.

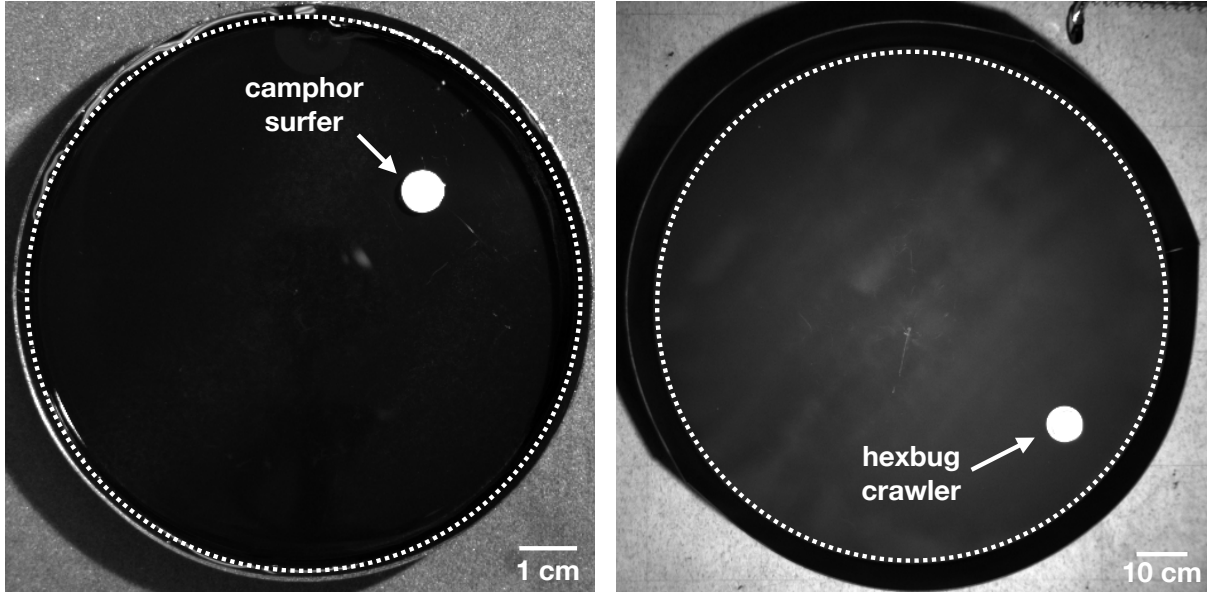


FIG. S1: Representative images of camphor surfer (left) and hexbug crawler (right)

NUMERICAL MODEL

For modelling the dynamics of both, surfers and crawlers, we consider the following stochastic dynamics for the translational and rotational degrees of freedom

$$m\ddot{\mathbf{r}} = -\gamma\dot{\mathbf{r}} + \gamma v_0 \mathbf{n} + \mathbf{f} \quad (\text{S1})$$

$$I\ddot{\varphi} = -\gamma_R\dot{\varphi} + \gamma_R\sqrt{2D_r}\eta \quad (\text{S2})$$

In Eq. (S1), $\mathbf{r} = (x(t), y(t))$ is the position of the center of mass of the macroscopic disc at time t . m is the mass of the disc, I the moment of inertia, γ and γ_R the translational and rotational friction coefficients. The moment of inertia is due to the fact that in the underdamped regime we have to take into account also the finite size of the particle. The particle is self-propelled along the direction given by the vector $\mathbf{n} = (\cos \varphi(t), \sin \varphi(t))$. v_0 is the self-propulsion speed, η is a random noise that satisfies $\langle \eta \rangle = 0$ and $\langle \eta(t)\eta(s) \rangle = \delta(t-s)$, and D_r is the rotational diffusion coefficient. In writing Eq. (S1), we consider as negligible the random fluctuations acting on translational degrees of freedom. This is

motivated by the fact that, in our experiments, the self-propulsion is the leading stochastic force acting on the system, i. e., the diffusion due to the thermal bath is orders of magnitude smaller than the random displacement due to the self-propulsion. Since we are considering the system confined by a circular container, \mathbf{f} is the force exerted by the boundaries on the particle. In particular, the boundaries are modelled using image particles located at a behind the confining structure [S35], where a is the size of the image. The image particle is thus modeled through a conservative central potential $\phi(r) = (A/r)^{12}$ with A a coupling constant that fixes the equilibrium distance between the particle and the wall. We consider a circular container of radius R .